JGR Atmospheres

RESEARCH ARTICLE
10.1029/2022JD037161

Record Arctic Cyclone of January 2022: Characteristics, Impacts, and Predictability

Edward Blanchard-Wrigglesworth[1], Melinda Webster[2,3], Linette Boisvert[4], Chelsea Parker[4,5], and Christopher Horvat[6,7]

[1]Department of Atmospheric Sciences, University of Washington, Seattle, WA, USA, [2]Geophysical Institute, University of Alaska Fairbanks, Fairbanks, AK, USA, [3]Polar Science Center, Applied Physics Lab, University of Washington, Seattle, WA, USA, [4]NASA Goddard Space Flight Center, Greenbelt, MD, USA, [5]ESSIC, University of Maryland, College Park, MD, USA, [6]Auckland University, Auckland, New Zealand, [7]Brown University, Providence, RI, USA

Key Points:

- A record low sea level pressure cyclone was observed in the Arctic in January 2022
- This low resulted in a record weekly loss of sea ice cover and record surface wind speeds, despite non-record warm conditions
- While the storm was well predicted, the rapid decreases in sea ice thickness and area were not

Supporting Information:

Supporting Information may be found in the online version of this article.

Correspondence to:

E. Blanchard-Wrigglesworth, edwardbw@uw.edu

Citation:

Blanchard-Wrigglesworth, E., Webster, M., Boisvert, L., Parker, C., & Horvat, C. (2022). Record Arctic cyclone of January 2022: Characteristics, impacts, and predictability. *Journal of Geophysical Research: Atmospheres*, *127*, e2022JD037161. https://doi.org/10.1029/2022JD037161

Received 20 MAY 2022
Accepted 17 OCT 2022

Abstract Arctic cyclones are a fundamental component of Arctic climate, influencing atmospheric heat and moisture transport into the region and surface energy, moisture, and momentum fluxes. Arctic cyclones can also drive changes in sea ice and energize ocean waves. Here we investigate a record low sea level pressure (SLP) Arctic cyclone which formed in East Greenland and tracked NE over the Barents and Kara seas between 21 and 27 January 2022. At its peak intensity on 24 January, the cyclone reached an estimated depth of 932.2 mb at 79.5°N 20°E. North of 70°N, this is the lowest SLP in the ERA-5 reanalysis over 1979 to present. The cyclone resulted in a record (over the period 1979–2022) weekly loss of regional sea ice area and surface wind speeds, and generated ocean waves exceeding 8 m that impinged on sea ice in the Barents sea, observed via satellite altimetry as large waves-in-sea ice up to 2 m in amplitude more than 100 km into the ice pack. Surface heat fluxes were strongly impacted by the cyclone, with record atmosphere-to-surface turbulent fluxes. However, the direct atmospheric thermodynamic impact on sea ice loss was modest, and the record sea ice changes were likely mainly driven by dynamical and/or ocean processes. While the storm was well predicted up to 8 days in advance, subsequent changes in sea ice cover were not, likely due to biases in the forecasts' sea ice initial conditions and missing physics in the forecast model such as wave-sea ice interaction.

Plain Language Summary The strongest recorded storm in the Arctic took place in January 2022. This storm was characterized by record wind speeds, sea ice loss and turbulent fluxes, and anomalous but less extreme temperature anomalies. We learned that some of this storm's record-breaking characteristics were predicted well by model forecasts. However, the effects of this storm on the Arctic sea ice cover were not well predicted. Forecasts underestimated the decrease in sea ice thickness and area from the storm. Satellite data showed large waves traveling into the icepack, which may have contributed to the sea-ice loss. Such processes may be poorly represented in the model, which hinder its ability to accurately forecast sea-ice conditions. Improving initial conditions and the representation of interactions between the atmosphere, sea ice, and ocean in models may help improve forecasts of weather and sea ice.

1. Introduction

Cyclones are fundamental to Arctic climate, impacting atmospheric heat and moisture transport into the region (e.g., Sorteberg & Walsh, 2008) and surface energy and moisture fluxes (e.g., Boisvert et al., 2016). Arctic cyclones can also force significant changes in sea ice (e.g., Clancy et al., 2022; Schreiber & Serreze, 2020) and ocean waves (e.g., Waseda et al., 2021), which can themselves break up sea ice (e.g., Asplin et al., 2012; Marko, 2003; Stopa et al., 2016) and may contribute to enhanced sea ice variability (e.g., Blanchard-Wrigglesworth et al., 2021). While the changing magnitude and frequency of Arctic cyclones under climate change is still a subject of debate (e.g., Neu et al., 2013), the reduction in the underlying sea ice cover with warming is likely to result in changes on the impacts of cyclones on Arctic sea ice, while changes in sea ice can themselves impact Arctic cyclones (e.g., Koyama et al., 2017). The predictability of Arctic cyclones shows reasonable skill, with current forecast models able to provide skillful predictions of cyclone location and depth up to 6 days in advance (Yamagami et al., 2018). On 21 January 2022, a cyclone formed over East Greenland before tracking in a NE direction and reaching an Arctic record-low depth of 932.2 mb east of Svalbard at 79.5°N 20°E on 24 January. The cyclone was accompanied by a record weekly loss of sea ice area (SIA) for the month of January in the Barents/Kara/West Laptev seas, a region that is a key contributor to pan-Arctic winter sea ice variability. Extreme events such

as this offer an opportunity to test our predictive models and understanding of underlying mechanisms that lead to erroneous predictions. In this paper, we characterize the record January 2022 Arctic cyclone, its atmospheric features, its impact on the ocean wave state and sea ice conditions, and the predictability of the cyclone and its impacts on sea ice.

2. Data

For atmospheric and ocean wave variables over 1979–2022 we use the ERA-5 reanalysis (Hersbach et al., 2020) at hourly and 0.25° resolution. We use the Melbourne University Cyclone Tracking Scheme (Simmonds et al., 2008; Webster et al., 2019) to track the January 2022 and previous extreme cyclones. Given higher uncertainty in reanalysis estimates of radiative variables (e.g., Lindsay et al., 2014), we also use satellite estimates of radiative fluxes at the surface (longwave) from NASA's Clouds and Earth's Radiant Energy System 1° resolution (CERES) CERES-SYN1DEG product, available over 2001–2022 (Wielicki et al., 1996), and turbulent fluxes (latent and sensible) derived from NASA's Atmospheric Infrared Sounder (AIRS) instrument, available over 2003–2022 (Susskind et al., 2014) at a 25 km resolution using the bulk aerodynamic method which has been adapted for areas covered with sea ice (e.g., L. N. Boisvert et al., 2013; L. Boisvert et al., 2015; Taylor et al., 2018). Uncertainties in AIRS-derived turbulent fluxes are 20% (Taylor et al., 2018), while uncertainties in the CERES derived net longwave over Arctic sea ice is around ∼20 W/m^2 (Huang et al., 2022). For sea ice concentration (SIC) observations, we use daily 25 km resolution SIC from the National Snow and Ice Data Center (NSIDC) near real time product for January 2022, and the climate data record version of satellite-derived observations of daily SIC from the NSIDC passive microwave data set (Meier et al., 2013) from 1979 to 2021. We calculate SIA by multiplying SIC with individual grid-cell areas and then summing over a region. For sea ice thickness up to a depth of approximately 1 m we use ESA's Soil Mapping Observing System (SMOS) level 3 sea ice thickness product at a 12.5 km resolution (Kaleschke et al., 2012; Tian-Kunze et al., 2014). To detect waves-in-sea ice using the ICESat-2 altimeter, we follow the methodology in Horvat et al. (2020) and utilize the L3A along-track sea ice height and type version 5 product (ATL07, Kwok et al., 2020) derived from Level 2A ATL03 photon heights (Neumann et al., 2019). The precision of sea ice height retrievals from ICESat-2 is about 2 cm (Kwok et al., 2019). For forecast output of both atmospheric and sea ice variables we use the ECMWF high-resolution (9 km) operational 10-day deterministic forecasts from its current IFS Cycle 47r3 model version. We focus on the ECMWF's forecast model for two reasons: Its Arctic atmospheric forecasts are consistently the highest skilled forecasts among global operational forecasts (Yamagami et al., 2018), and its current version includes sea ice forecasts derived from a sea ice model (the LIM3 model, Rousset et al., 2015).

3. Results

Figure 1 shows sea level pressure (SLP), SIC, significant wave height and direction at the time of the cyclone's peak intensity on 13 UTC 24 January 2022, together with the monthly minimum hourly SLP value over 1979–2022 (for all months) in ERA5 north of 70°N and 80°N. SLP reached a minimum value of 932.2 mb at 79.25°N 37.75°E just to the east of Svalbard and over sea ice cover (SIC >80%, Figure 1a). Large waves greater than 8 m in height are observed over the open ocean, with the swell direction propagating toward the sea ice edge over most of the Barents Sea (Figure 1b). The estimated SLP minimum value is the lowest SLP value in the ERA-5 reanalysis north of 70°N over its full record (January 1979 to March 2022, Figure 1c), surpassing the previous record of 933 mb from December 1990. Even more noteworthy is the northern latitude of the January 2022 low at its peak intensity—over the 80°N–90°N domain, the lowest SLP value of the January 2022 cyclone was 933.4 mb, significantly lower than the previous minimum SLP record over this domain of 938 mb from January 2002 (Figure 1d). Inspecting minimum SLP values over both domains shows no trends over 1979–2021, suggesting that recent climate change has not resulted in lower SLP extreme cyclones over the Arctic. Figure S1 in Supporting Information S1 shows the timeseries of the January 2022 cyclone's minimum SLP throughout its lifetime over 21–28 January, its storm track, and the storm track of the previous 10 record low SLP Arctic cyclones north of 70°N.

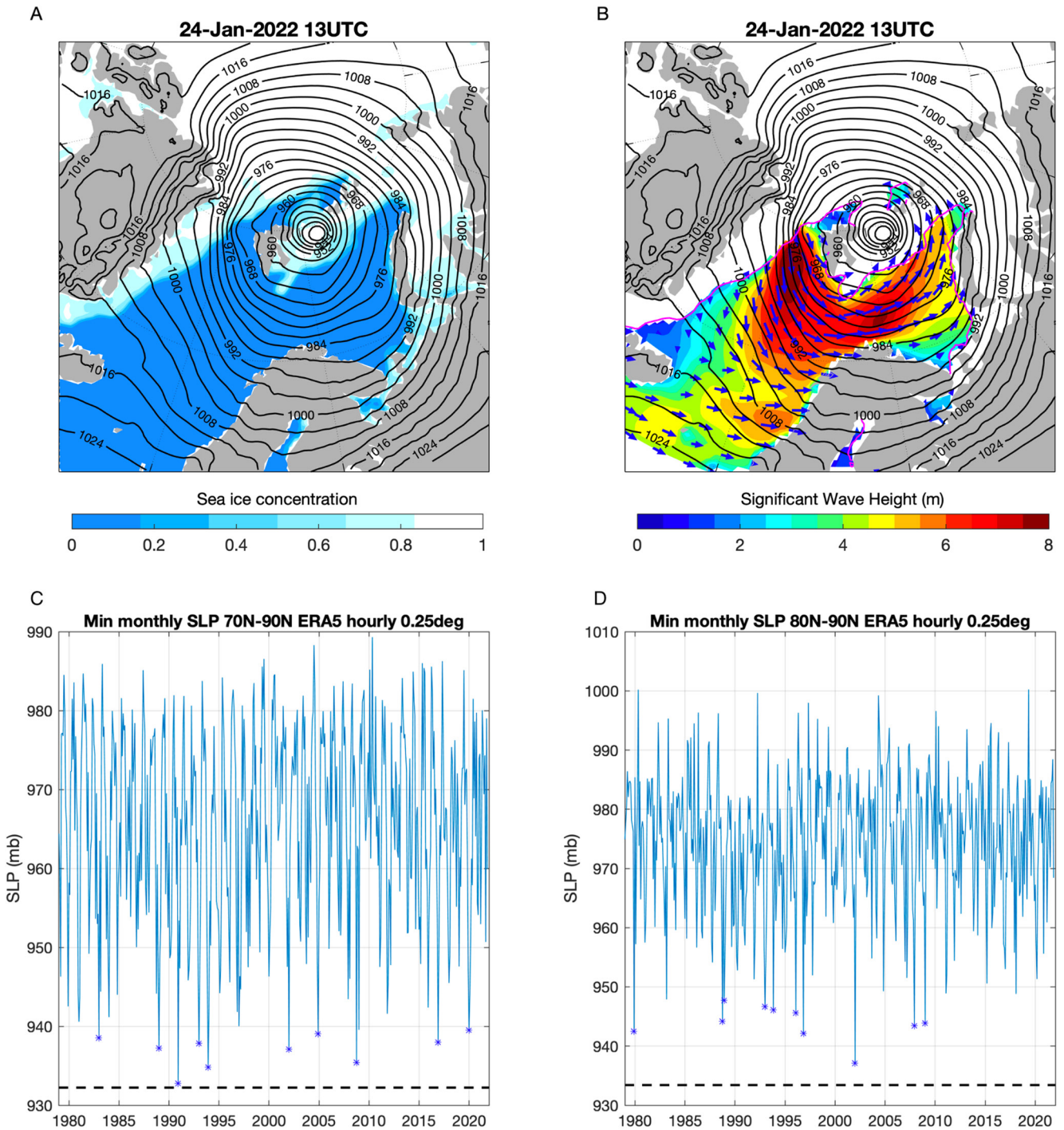

Figure 1. Conditions on 24 January at 13:00 UTC, showing SLP (contours) and SIC (shading), panel (a) and significant wave height and direction (panel b). Monthly minimum hourly SLP over 70°N–90°N and 80°N–90°N (panels c and d) for all months, January 1979–January 2022. The minimum values during the January 2022 cyclone are shown by the dashed horizontal lines in (c and d). The asterisks denote the 10 extreme cyclones in each domain prior to January 2022.

3.1. Cyclone Evolution 19–28 January 2022

Figure 2 shows daily (at 12UTC) values of SLP, windspeed, and the sea ice edge (defined by the SIC = 15% concentration threshold) over 20–28 January, and six-hourly from 23 January 12 UTC to 24 January 12 UTC, the period leading to the cyclone's peak intensity and minimum SLP. In Figures S2 and S3 in Supporting Information S1 we show the equivalent analysis for significant wave height, wave direction, and 300-hPa winds.

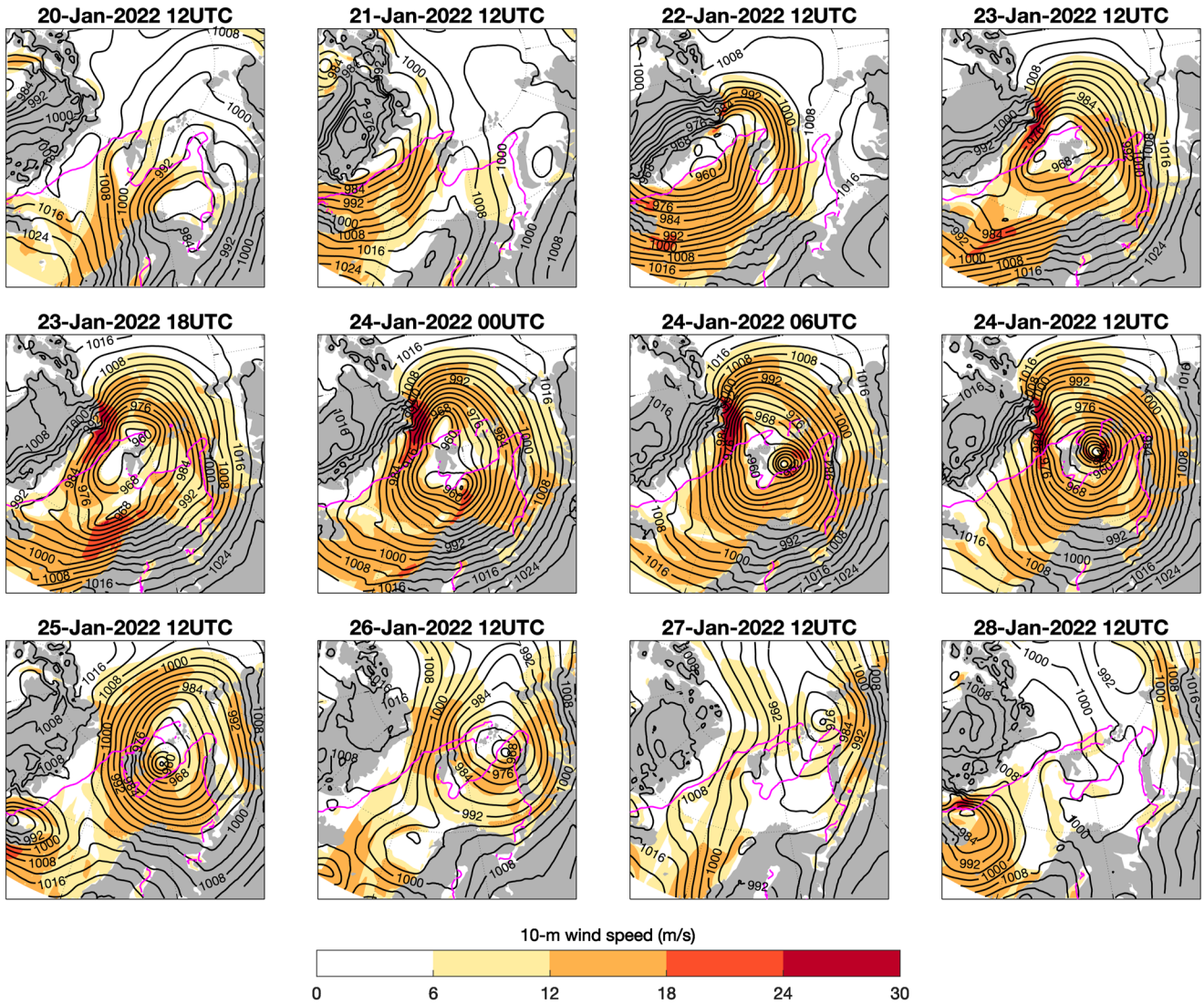

Figure 2. SLP (contours), 10-m wind speeds (colored shading) and 15% SIC contour (magenta), 20–28 January 2022.

Figure 3 shows the potential temperature on the 2 PVU surface and SLP from 19 January to 24 January. While the cyclone tracking only detects the formation of the closed low on 21 January over Greenland (Figure S1 in Supporting Information S1), Figure 3 shows that on 19 January, a surface low was present over the Labrador/Baffin bay region. On 20 January, SLPs over the East Greenland sea were 1,010–1,015 mb (Figure 2) with an upper level ridge aloft (Figure 3) around which a strong zonal jet set over East Greenland (Figure S3 in Supporting Information S1). On the same day, to the west and southwest, an upper level trough with a coherent feature characteristic of a weak tropopause polar vortex (TPV, e.g., Hakim & Canavan, 2005; Cavallo & Hakim, 2009) approached southern Greenland and a surface low started developing off southernmost Greenland between 20 and 21 January (Figure 3). While SLP values over Greenland need to be assessed with caution (given the high surface elevation), the upper level trough and the surface low over the Labrador on 19/20 January likely played a role in the development of the quickly deepening low over the East Greenland Sea by 21 January (SLPs around 970 mb), perhaps also aided by lee cyclogenesis supported by the upper level jet over East Greenland during 20 January. The low on 21 January over the East Greenland sea subsequently drifted NE over the next two days, with a central pressure that oscillated around 955–960 mb and generally tracked the sea ice edge (Figure 2). On 23 January, a secondary low started to develop to the east of Iceland, supported by a strong upper level jet (Figure S3 in Supporting Information S1) and a well-defined upper level vorticity anomaly (likely a TPV which can be tracked back to at least January 19, labeled with a magenta X in Figure 3). This secondary low quickly intensified

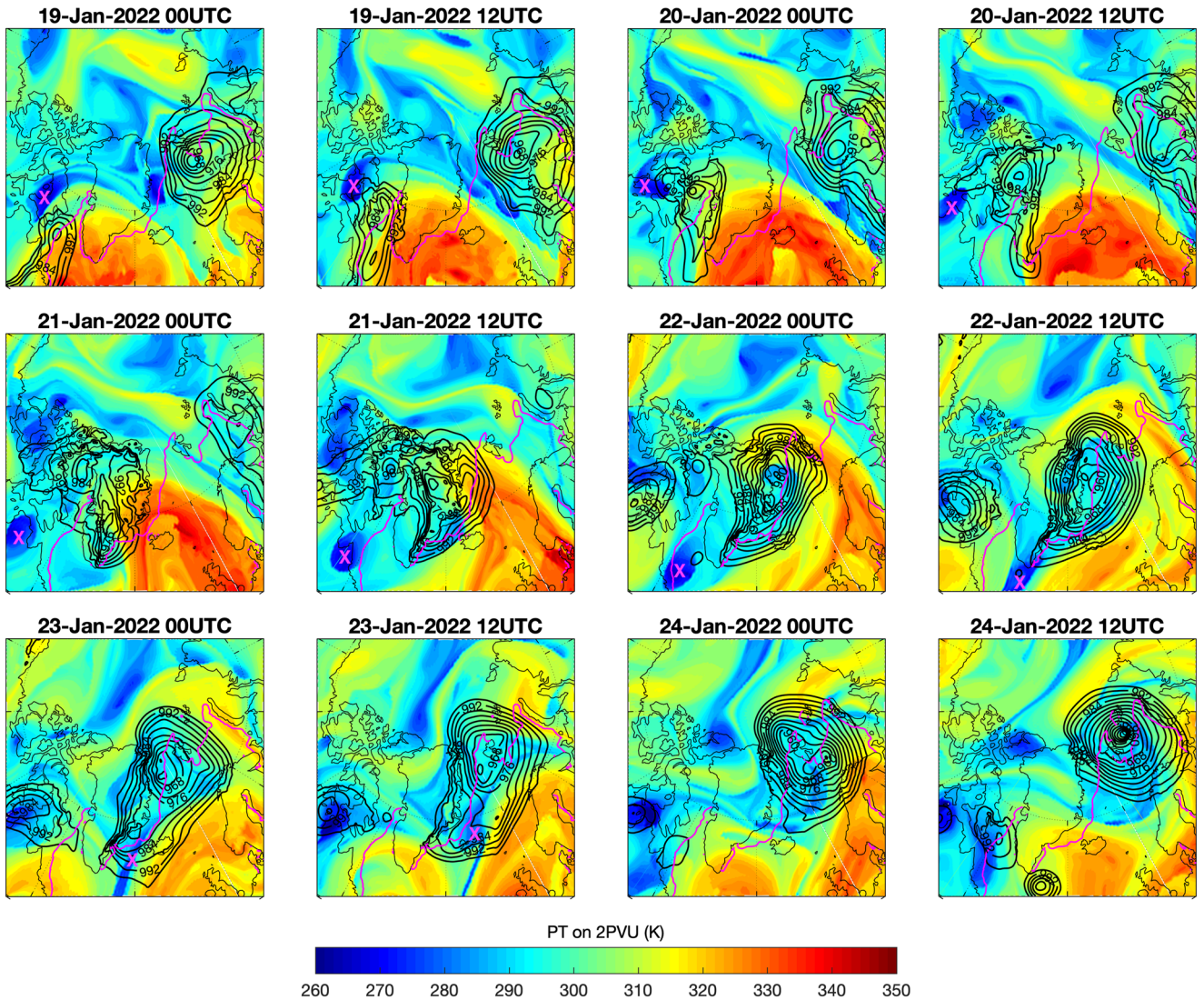

Figure 3. Potential Temperature on the 2 PVU surface (shading, in Kelvin), SLP (black contours, for clarity only plotted for SLP values below 1,000 mb), and 15% SIC contour (magenta), 19–24 January 2022. The magenta X labels the upper level TPV that interacts with the secondary cyclone formation during 23 January.

and traveled NE, and during 24 January was entrained within the main circulation and became the principal low of the cyclone system. After reaching its lowest pressure at 13 UTC 24 January, the low quickly filled in and by 26 January reached an SLP value of 960 mb and kept traveling in a ENE direction (Figure 2). On 28 January the low exited the region via the northern Laptev Sea, filling in to 995 mb, and dissipated completely by 29 January. Based on results from the cyclone Tracking Scheme (Simmonds et al., 2008; Webster et al., 2019), the previous 10 record low cyclones north of 70°N all occurred in the Atlantic and Nordic sea region (Figure S1 in Supporting Information S1), with cyclone formation generally occurring over the ocean.

During the lifetime of the cyclone, surface wind speeds were regularly over 12 m/s over the ocean and sea ice, peaking during 23–24 January over the Fram Strait and over the northern Barents sea to the south and east of the cyclone low, where winds were in excess of 24 m/s (Figure 2). The largest 1 hr wind speeds over the Barents Sea reached 28 m/s (100 km/hr) on 24 January, which for the location was a record maximum wind speed in ERA-5 for all months over 1979–2022 (Figure S4 in Supporting Information S1).

3.1.1. Temperature and Surface Fluxes

Figure 4 shows the surface (2 m) air temperature together with the SLP and sea ice edge for 20–28 January (Figure 4a), along with the timeseries of the average temperature over a Barents Sea domain (averaged over

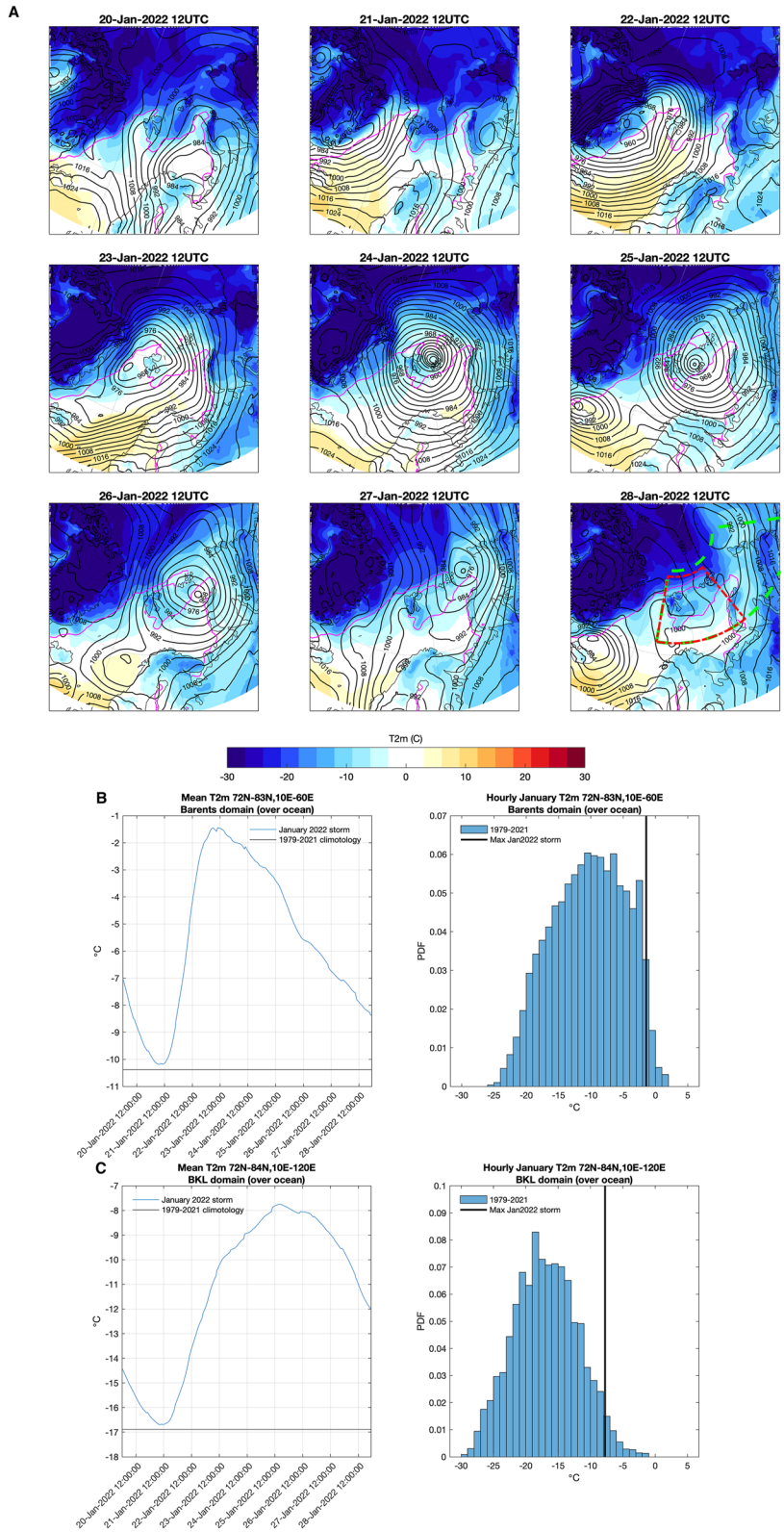

Figure 4. SLP (contours) and surface temperature (shading), 20–28 January 2022 (top panel) and evolution of the mean temperature in the Barents Sea and BKL domain (shown in the red and green dashed boxes, note that the western and southern boundaries of the Barents Sea overlap with the BKL domain boundaries) with a PDF of January 1979–2021 hourly temperatures for those domains, highlighting the maximum value during the January 2022 storm with the black vertical lines. The thin horizontal lines represent the January 1979–2021 climatology for the domains.

72°N–83°N and 10°E−60°E, Figure 4b) and a larger Barents/Kara and western Laptev Sea (BKL) domain (averaged only over the ocean domain over 72°N–84°N and 10°E−120°E, Figure 4c), and the histogram of hourly January temperatures for these domains in the ERA-5 record over 1979–2021. Figure S5 in Supporting Information S1 shows the surface air temperature anomalies with respect to the 1979–2021 January climatology. Temperatures in the region were close to climatology during 20–21 January, before quickly rising on 22 January as the cyclone approached and south/southwesterly flow set up over the region. Temperatures in the Barents Sea peaked to just below freezing on 23 January (Figures 4a and 4b) and temperature anomalies were widely over 10°C warmer than average over the sea ice covered regions in the north Barents, Kara, and Laptev seas (Figure S5 in Supporting Information S1). From 24 January onward a slow cooling trend set up in the Barents Sea as the cyclone traveled in a E/NE direction and northerly flow returned to the Barents Sea, yet temperatures remained anomalously warm further east over the Kara and western Laptev seas until 28 January (Figures 4a and 4c). While temperatures averaged over the Barents Sea and the wider BKL domain were about 9°C above climatology at their peak they were not record-breaking—the record maximum 1979-2021 January temperatures are 2°C in the Barents region and −8°C in the BKL domain, and the maximum January 2022 value is around the 95th percentile of the 1979–2021 temperature distribution (Figures 4b and 4c). Figure S6 in Supporting Information S1 shows the same analysis as Figure 4 for 850 hPa temperatures which show a similar pattern.

Following Boisvert et al. (2016), we next focus on the net longwave (NLW) and turbulent (sensible plus latent) fluxes, and the net surface energy budget (SEB), defined as:

$$F_U + F_s + F_l - F_r - F_L = \text{SEB}, \tag{1}$$

$$F_U - F_L = \text{NLW}, \tag{2}$$

where F_U is the upwelling (emitted) longwave radiation, F_s and F_l are the sensible and latent heat fluxes, F_r is the net shortwave radiation and F_L is the downwelling longwave radiation respectively (negative values denote into the surface from the atmosphere, and therefore ocean/sea ice warming). Shortwave fluxes are negligible in January in this region and are omitted from the analysis. Figure 5 shows the daily mean SEB and individual fluxes averaged over the Barents/Kara/West Laptev region (over 72°N–84°N and 10°E−120°E, averaged only over the ocean domain where mean SIC over 21–27 January 2022 is greater than 50%) for 20–28 January and for the 2003–2021 climatology for these dates as estimated both in ERA-5 and satellite (CERES and AIRS, Figures 5a and 5b), and the anomalous (with respect to climatology) fluxes (Figures 5c and 5d). Using ERA-5, climatological January SEB fluxes are ∼60 W/m^2, partitioned into ∼40 W/m^2 in the net longwave and ∼10 W/m^2 each in the latent and sensible fluxes (Figure 5a). The cyclone resulted in reduced fluxes from the surface to the atmosphere. On 23 January, the SEB was around zero, and the 21–27 January average was ∼23 W/m^2 (an anomaly of ∼−37 W/m^2). The anomaly was dominated by the sensible fluxes (about ∼−20 W/m^2), followed by the longwave and latent (∼−15 W/m^2 and ∼−5 W/m^2 respectively). Using CERES/AIRS, climatological January SEB fluxes are close to zero (∼3 W/m^2), which results from ∼31 W/m^2 in the net longwave and ∼−28 W/m^2 in the turbulent fluxes (Figure 5b). Turbulent fluxes from the atmosphere to the surface peaked over 24–26 January, when turbulent heat fluxes reached ∼−90 W/m^2 (an anomaly of ∼−60 W/m^2). Longwave fluxes during the cyclone are about ∼25 W/m^2, an anomaly of ∼−7 W/m^2 with respect to climatology.

Comparing the anomalous fluxes in Figure 5 shows better agreement between ERA-5 and CERES/AIRS (Figures 5c and 5d). The total SEB anomaly is strongly negative during the cyclone, peaking ∼−60 W/m^2 in both datasets. The mean SEB anomaly during 21–27 January is ∼−35 W/m^2 in both datasets, and is mostly driven by the anomaly in the turbulent fluxes, while the anomaly in the net longwave flux accounts for a slightly larger role of the total 21–27 January SEB anomaly in ERA-5 compared to CERES/AIRS.

Inspecting the 6-day running means for the turbulent, net longwave and total SEB fluxes in both ERA-5 and CERES/AIRS for January shows that the turbulent fluxes during the January 2022 cyclone were more extreme than the net longwave radiation (cf. Figures 6a and 6b, Figures 6d and 6e), and both the 6-day mean turbulent flux and total SEB fluxes over 22–27 January 2022 were the most negative in CERES/AIRS over 2003–2022 (average of −71 W/m^2 and −45 W/m^2, respectively). The more extreme character of turbulent fluxes compared to longwave fluxes during the cyclone may be due to the combination of the anomalous (but not as extreme) air temperatures (which dominate longwave fluxes) with the extreme surface winds (which enhance surface turbulent fluxes) that characterized the cyclone.

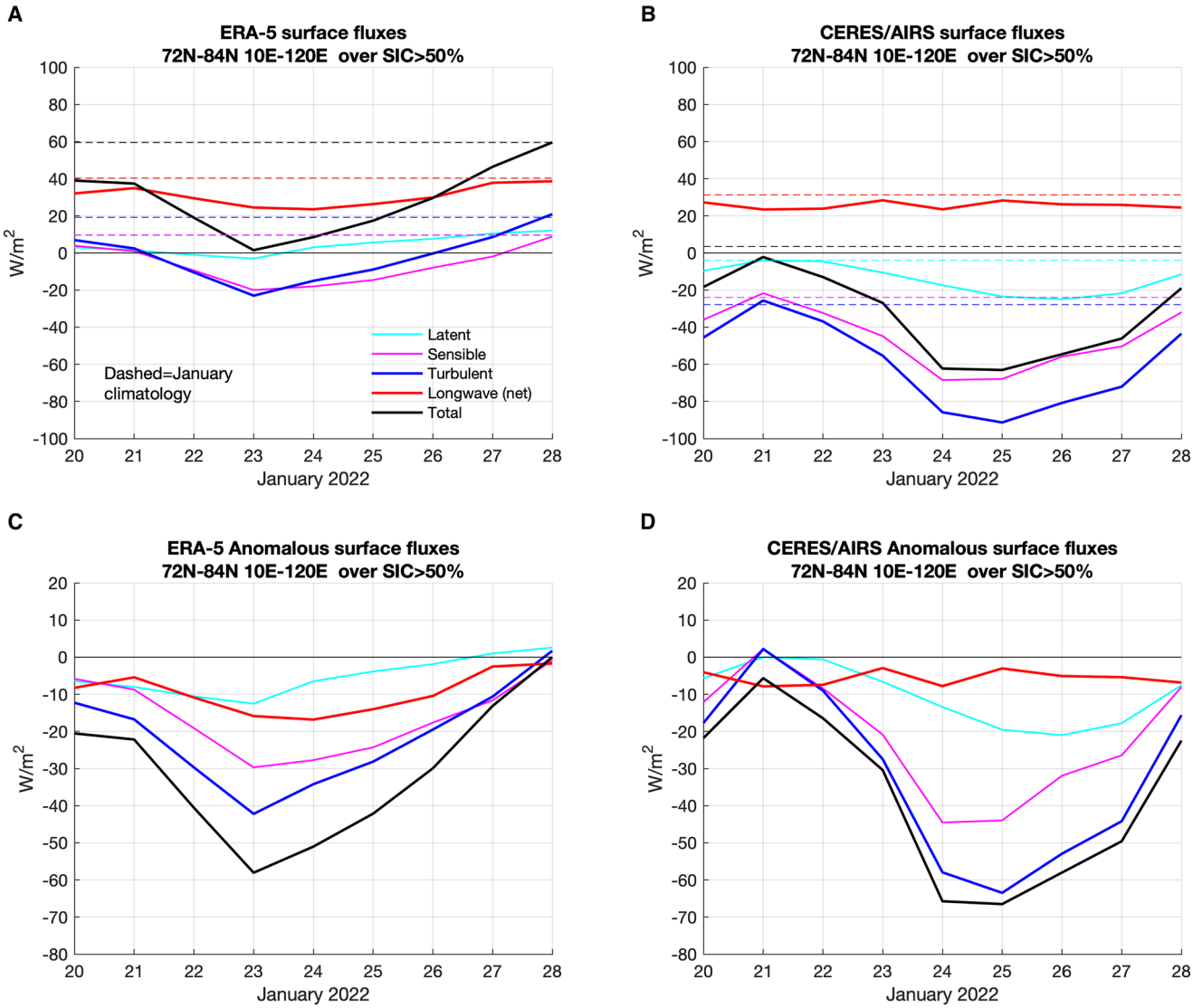

Figure 5. Daily turbulent, net longwave and total SEB surface fluxes from 21 January 2022 to 28 January 2022 and for the 2003–2022 January climatologies (shown dashed) in ERA-5 (left panels) and CERES/AIRS (right panels). Values shown are area-weighted means for the BKL region for 72–84°N and 10–120°E over the ocean domain where SIC is greater than 50% over 21–27 January 2022. Top panels show absolute values and bottom panels show anomalous values. Negative values denote into the surface from the atmosphere.

3.2. Ocean Wave and Sea Ice Impacts

Figure S2 shows that the cyclone produced a large swell by 22 January just east of the East Greenland Sea, associated with strong surface southwest winds shown in Figure 2. Over the following 2 days the swell propagated in a northeasterly direction toward the Barents Sea, supported by continued southwest winds. In addition, a second wave group grew in the Barents Sea on 23 January, a result of strong surface winds over the Barents Sea associated with the incoming cyclone. Large wave heights persisted in the Barents Sea until 26 January, peaking at 8 m on 24 January. Waves have been previously observed to penetrate the sea ice pack during winter storms and can be detected using satellite altimetry (e.g., Horvat et al., 2020). NASA's ICESat-2 obtained a surface height retrieval from the sea ice covered Barents Sea region east of Svalbard on 23 January (Figure 7). Large (2 m) amplitude waves-in-sea ice were observed close to the sea ice edge at ~77°N, dampening in a south-to-north direction over 1° latitude (~100 km). The SIC over which the waves are observed is close to 100% SIC.

Figures 8 and 9 show SIC and thickness respectively at the beginning (21 January) and end (27 January) of the cyclone and the difference between the two dates. Figure 8 also shows the total SIA evolution in the BKL domain

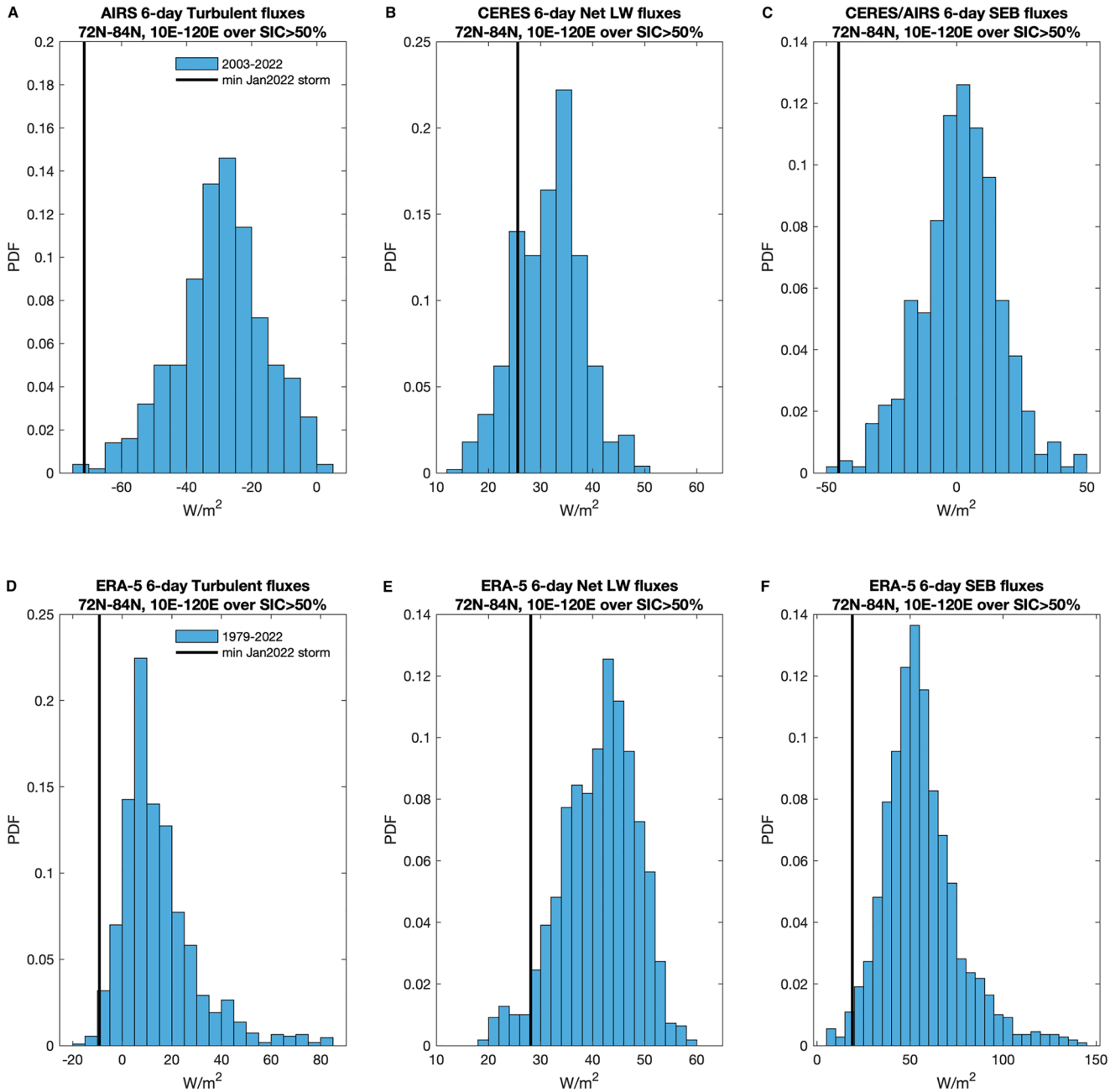

Figure 6. Histogram of 6-day mean turbulent fluxes (left panels), net longwave (middle panels) and SEB fluxes (right panels) over the BKL domain (72–84°N, 10–120°E over the ocean domain where SIC is greater than 50% over 21–27 January 2022) in CERES/AIRS over 2003–2022 (top row) and ERA-5 over 1979–2022 (bottom row), with the minimum 6-day mean values from January 2022 (which take place during the storm) in black.

and historical distribution of 6-day BKL SIA changes (defined as $SIA_d - SIA_{d-6}$ where d is day). On 21 January, SIC was close to the 1979–2021 climatology, in contrast to recent years which have generally shown reduced sea ice cover (Figure 8d). The northern Barents Sea was covered in sea ice, and a tongue of sea ice extended along the western coast of Novaya Zemlya. The Kara and Laptev seas had close to 100% sea ice coverage on this date (Figure 8a). By 27 January, sea ice cover had reduced drastically, especially in two areas, between northern Svalbard and Franz Josez, and along the sea ice edge to the north of Novaya Zemlya (Figures 8b and 8c). There was also significant sea ice loss along the western Laptev Sea and in the vicinity of southern Novaya Zemlya. Over large areas of the Kara and Barents seas SIC values dropped from close to 100% to 70%–80%. Sea ice area in the BKL domain, south of 84°N and between 10°E–110°E, dropped by over 0.4 million km^2 between 21 January

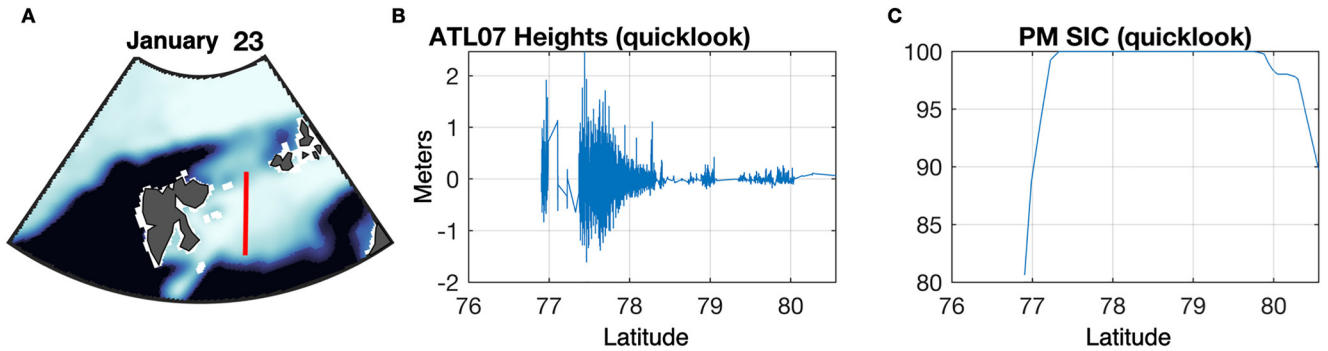

Figure 7. ICESat-2 retrieval on 23 January 2022 (left panel), with surface height in meters plotted against latitude (middle panel) and SIC (in %) along the ICESat-2 transect (right panel).

and 27 January (Figure 8d). This is the largest recorded 6-day SIA loss in January in this region over 1979–2022, and is 30% greater than the previous record 6-day January SIA loss (Figure 8e). Extending analysis of the 6-day SIA changes in the BKL domain throughout the year shows the extreme character of the January 2022 SIA loss (Figure S7 in Supporting Information S1 shows histograms of 6-day of BKL SIA, SIA anomaly, and normalized SIA changes throughout the year and in winter).

Sea ice thickness on 21 January was estimated to be thin in the Barents Sea (less than 1 m), while thicker ice over 1 m was common in the Kara and Laptev seas (Figure 9a). Sea ice thickness in the northern SIC loss region (between North Svalbard and Franz Josef) was thin on 21 January (mostly less than 0.5 m). By 27 January most of the region experienced a reduction in sea ice thickness (Figure 9b). To the east of Svalbard and Novaya Zemlya, there were remarkable reductions in sea ice thickness of up to 1 m, and even regions that did not experience a significant loss in SIC, such as the northern Kara Sea, experienced a thickness reduction of 0.25–0.5 m (Figure 9c). Considering the changes both in SIC and SIT over this period, this was a remarkable event of sea ice loss.

How much of the estimated sea ice thickness loss may be due to the thermodynamic forcing from the atmosphere? To answer this question we use the CERES/AIRS mean 21–27 January SEB fluxes of ~ -35 W/m^2 (note that the mean SEB fluxes in ERA-5 still imply a net loss from the surface to the atmosphere and thus no sea ice melt forced by the atmosphere) and following Boisvert et al. (2016), we use a simple thermodynamic approach to calculate the amount of sea ice melt caused by a negative SEB, given

$$\delta h = Q / (\rho * c_f), \tag{3}$$

where δh is the change in sea ice thickness, Q is the SEB, ρ is the density of sea ice (930 kg/m^3) and c_f is the latent heat of fusion of sea ice (3.2×10^5 J/kg). This simple approximation neglects sea ice heat capacity and assumes negligible heat conduction through sea ice, and thus can be used to estimate an upper bound of sea ice melt resulting from the SEB (i.e., sea ice is already at the melting point, and all the SEB goes to melting sea ice). For $Q = -35$ W/m^2, $\delta h = -0.87$ cm of ice per day. Thus, over the course of the cyclone, we might expect no more than ~ -5 cm of sea ice thickness change from thermodynamic forcing averaged over the BKL domain, a small fraction of the estimated sea ice thickness loss shown in Figure 9.

3.3. Predictability of the Cyclone and Sea Ice Impacts

The above analysis shows that the January 2022 cyclone was an extreme event, both in terms of atmospheric dynamics (SLP and surface winds) and its impacts on sea ice and ocean waves. We next investigate the predictive capability of the state-of-the-art ECMWF high resolution operational model on the cyclone and its impacts on sea ice.

Figure 10 shows the 0–8 days leadtime forecasts of SLP and surface wind speed for 24 January 12UTC, and Figure 11 shows the 0–10 days leadtime forecasts of minimum SLP and maximum windspeed in the vicinity of the 24 January 12UTC cyclone center (76°N–82°N, 15°E–45°E, Figures 11a and 11b), area-averaged 2 m air temperature over the Barents Sea and the BKL domain (Figures 11c and 11d), and the forecast central low position

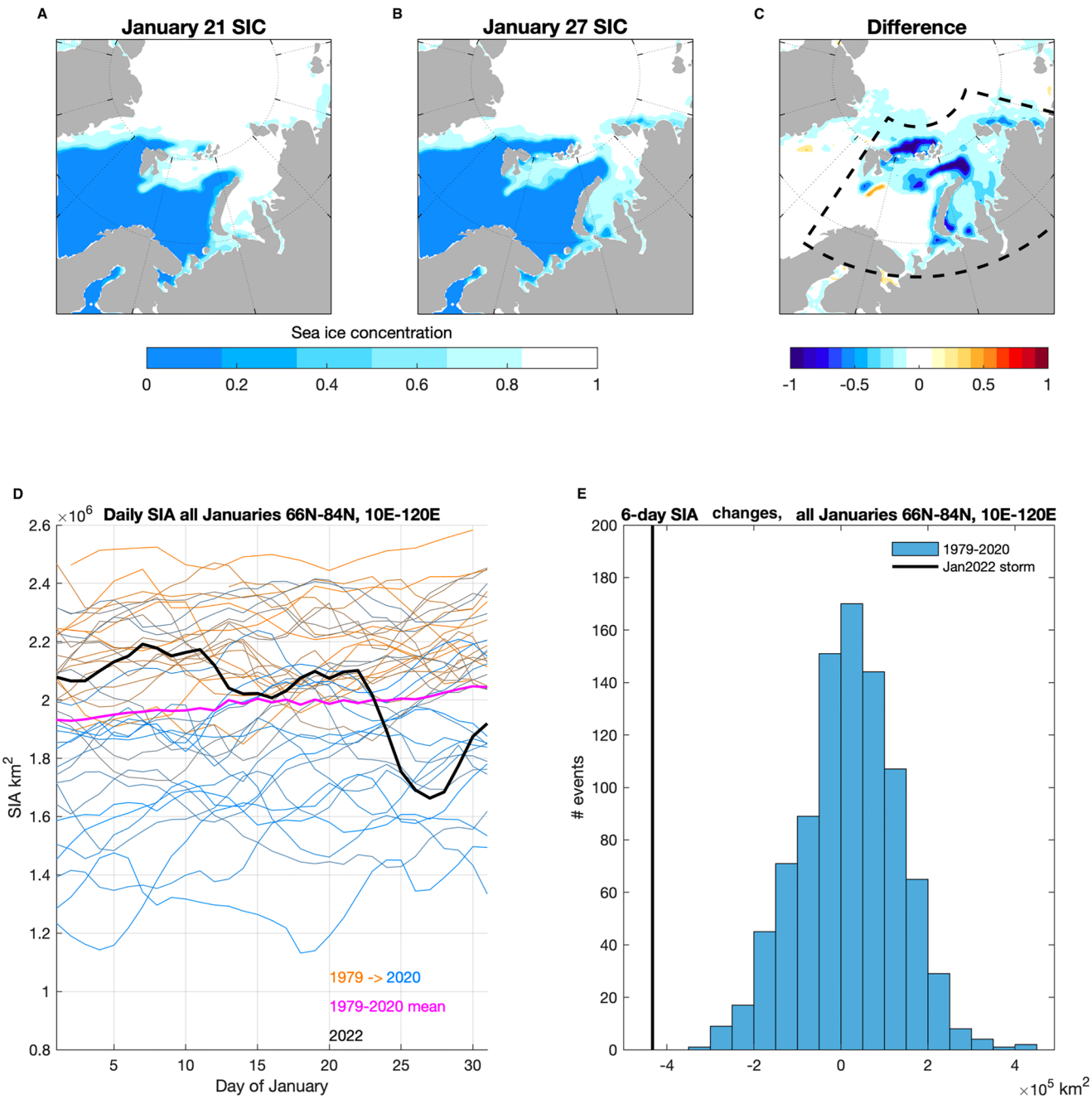

Figure 8. Observed sea ice concentration on 21 January 2022, 27 January 2022, and the difference (top row), total SIA in the BKL domain (shown by the black dashed box) January timeseries over 1979–2022 (bottom row left panel), and histogram of historic 6-day changes over 1979–2021 for all Januaries using the full month to calculate the SIA changes (bottom row right panel).

and pressure error metrics (Figure 11e, following the approach in Yamagami et al., 2018). The 10-to-6 days forecasts were skilled in forecasting a deep cyclone on 23-24 January in the vicinity of the northern Barents Sea, but the forecasts of the low pressure's minimum were too high (forecast low of 950–960 mb) and the surface winds too weak (Figure 10). Central position errors of the cyclone at these leadtimes are around 400–800 km (Figure 11e). The timing of cyclone evolution for these 10-to-6 days forecasts also tends to be slightly earlier, with minimum SLP values forecast for 23 January (Figure 11a). At 5 days and shorter leadtimes, the forecasts gain skill and slowly converge toward the observed state, forecasting a deep cyclone and strong surface wind speeds in the Fram Strait and in the south and east vicinity of the low, with remarkably skillful central position errors

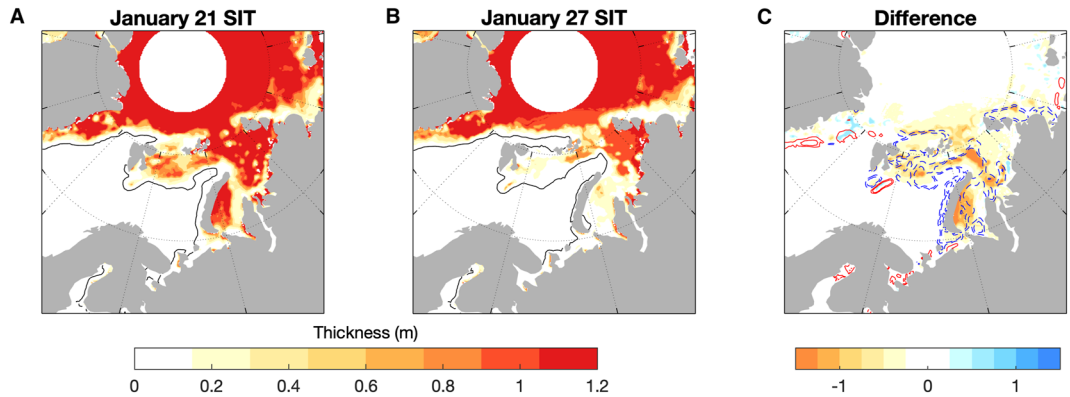

Figure 9. As shown in Figures 8a–8c, but for sea ice thickness. The black contours in panels (a and b) show the 15% SIC contour for the date, and the blue and red contours in (c) show the 15% and 30% SIC losses and gains respectively between the two dates. The white area around the North Pole is outside the satellite's sampling domain.

(<300 km, Figure 11e) and central pressure errors (<15mb). Forecasts of peak wind speeds however tended to be biased low for forecasts initialized earlier than January 23 (Figure 10b). Forecasts of mean Barents Sea and BKL domain 2 m air temperatures were rather skilled in forecasting the initial warm-up during 22 January, but tended to cool down too quickly thereafter (Figures 11c and 11d). Overall, the forecast model shows remarkable skill in forecasting a significant cyclone particularly at lead times of 5 days or less. The skill of the January 2022 forecast in terms of central position and pressure is comparable or better than the forecast skill for summer Arctic cyclones, which is >500 km and 10–15 mb for 5-day leadtimes (see Figure 4 in Yamagami et al., 2018).

Figure 12a shows 0–10 days forecasts initialized over 14-24 January of SIA in the Barents/Kara/East Laptev domain. Forecasts show a SIA loss between 21 January and 27 January of about 0.2 million km^2 from 2.1 million km^2 to about 1.9 million km^2, about half of the observed loss (Figure 8), and a small recovery in SIA after 27 January. As most of the observed SIA loss took place between 22 January and 27 January, we focus on forecasts initialized on 21 January. Figure 12b shows SIC on 21 January (0 days leadtime) and its forecast of 27 January (6 days leadtime). While the initialized SIC is close to observations (Figure 8a), the forecast for 27 January shows more extensive sea ice cover than observed (Figure 8b), with high SIC values between north Svalbard and Franz Josez. The forecast captures the spatial pattern in the observed SIC loss, as shown by the SIC differences between 21 and 27 January (Figures 8 and 12c) along the Barents Sea ice edge, in the southern vicinity of Novaya Zemlya, and along the western Laptev Sea coast, albeit with a smaller amplitude. In contrast, the observed SIC loss along north Svalbard to Franz Josez is not forecast. Figure 12c shows sea ice thickness from the same forecast. On 21 January, sea ice thickness tends to capture the large scale patterns in observations (Figure 9a), but is too thick in the Barents Sea. The forecast for 27 January shows mostly small changes in sea ice thickness between the two dates. While there is a region of larger forecast SIT loss just NE of Novaya Zemlya, these forecast changes are much smaller than the observed estimates in SIT change in Figure 9c.

4. Discussion and Conclusions

An extreme Arctic cyclone developed over Greenland and tracked NE into the Barents Sea and high Arctic over 20–28 January 2022. At its peak intensity, the central pressure reached an estimated 932.2 mb, the lowest hourly SLP value in the ERA-5 reanalysis north of 70°N over 1979–2022.

The cyclone had significant impacts on the atmosphere, sea ice and ocean waves. Air temperatures at the surface and aloft peaked over 10°C above climatology over large sections of the Barents/Kara/East Laptev seas, accompanied by extreme surface winds, with 1-hourly values that peaked at 100 km/hr over the north Barents Sea. Surface energy fluxes were also anomalous with respect to climatology, with a mean 6-day net input of energy into the sea ice from the atmosphere of ~35 W/m^2 as estimated using satellite data, dominated by extreme turbulent fluxes, which were the largest for January over 2003–2022. While the SEB values are anomalous, they are smaller than the ~60 W/m^2 estimated for the extreme cyclone of December 2015/January 2016 in the Barents/Kara seas, an event that was dominated by extreme warmth and moisture anomalies (Boisvert et al., 2016). The January 2022

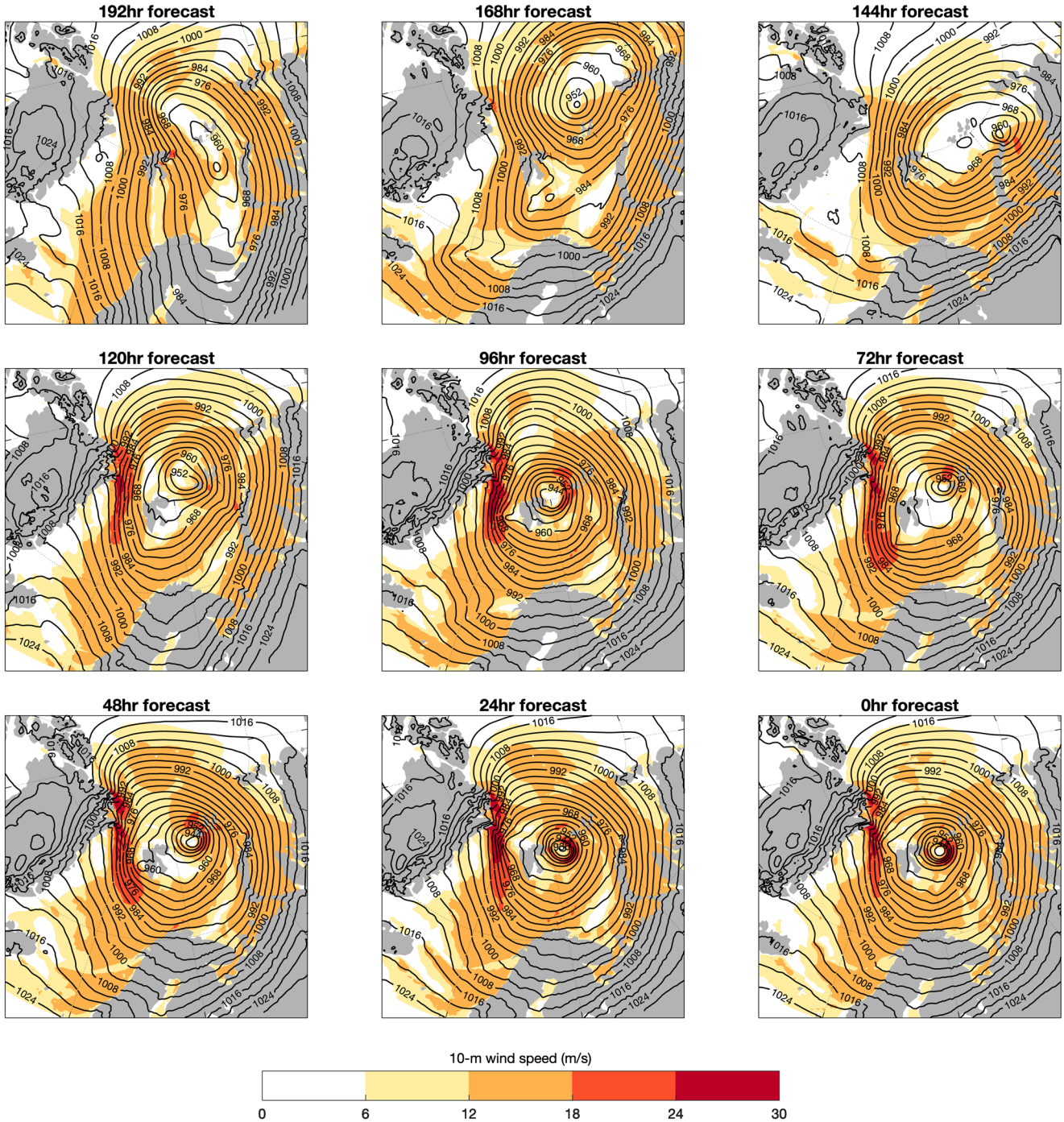

Figure 10. SLP and surface wind forecasts of 24 January 12UTC at 0–8 days (192 hr) leadtimes.

cyclone temperature anomalies were also not record values, but were in the 95% percentile. Surface wind speeds reached record values over a sea-ice covered sector of the Barents Sea, and large ocean waves over 6 m impinged on the sea ice over several days, with significant waves-in-sea-ice of 2 m height detected by satellite altimetry up to 100 km into the sea ice pack.

The sea ice cover was heavily affected by the cyclone, and the 6-day SIA loss in the region of 0.4×10^6 km^2 was the most extreme January SIA loss over 1979–2022, surpassing the previous record loss by 30%. Sea ice thickness was also strongly impacted, and over large regions sea ice thickness decreased by over 0.5 m. The losses in sea

Figure 11. Forecasts of SLP minimum and wind speed maximum in a domain centered around the 24 January 12UTC cyclone center (76°N–82°N, 15°E–45°E), panels (a and b), and forecasts of area-averaged 2 m-air temperature over the Barents Sea and the BKL domain (panels c and d). Observed values from ERA-5 are shown in black (top and middle rows). SLP forecast errors for 24 January 12 UTC as a function of leadtime, showing central pressure error (left axis) and central location error (right axis, panel e).

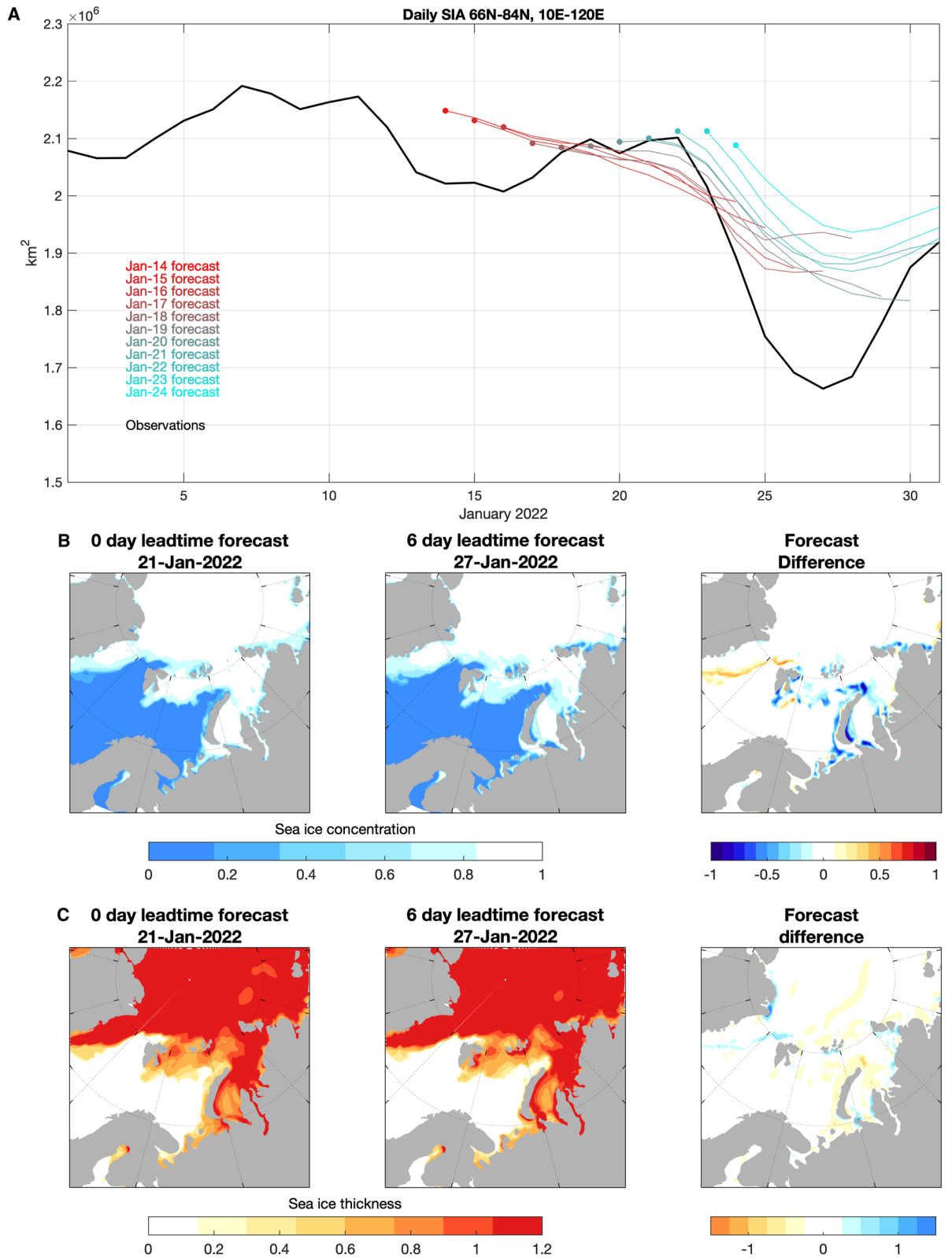

Figure 12. ECMWF forecasts and observed SIA in the BKL domain (A, top panel), forecasts of SIC (middle row) and SIT (bottom row) initialized on 21 January for 21 January (0 days leadtime) and 27 January (6 days leadtime) and the forecast differences between the two dates. Note that to be consistent with SMOS sea ice thickness, we do not differentiate sea ice thickness categories thicker than 1.2 m.

ice thickness are generally much larger than can be accounted for by the surface energy fluxes, which can only explain ~5 cm of melt averaged across the region using the satellite flux estimates. This suggests that sea ice dynamics and/or enhanced bottom melt due to upper ocean mixing were responsible for a significant amount of sea ice loss, agreeing with previous studies of winter cyclones and their impact on sea ice in this region that have highlighted the role of dynamics in driving sea ice loss (Park et al., 2015). The role of the large waves in sea ice loss and their ability to break sea ice and mix heat vertically in the upper ocean is also unknown. We find no trend over 1979–2021 in minimum SLP over 70°N–90°N, and 80°N–90°N domains, suggesting that the January 2022 cyclone event is, at least from an atmospheric dynamics perspective, unrelated to recent climate change. However, its impacts on the sea ice may have been larger because of recent climate trends, as the large loss in sea ice cover may have been pre-conditioned by thin sea ice prior to the cyclone.

Extreme events have an oversized footprint on socioeconomic impacts, but also serve as litmus tests for our environmental system models and their predictive capabilities, and thus the predictability of extreme events is of interest both in a scientific and social context. Our initial forecast validation of the January 2022 cyclone shows that, while the cyclone and accompanying strong winds and warm temperatures were reasonably well predicted especially at 5 days and shorter leadtimes, the changes in sea ice were not predicted with high skill, consistent with the low forecast skill of extreme sea ice change events in current-generation sub-seasonal to seasonal forecasting models (McGraw et al., 2022). Forecasts consistently underestimated the loss in SIA and sea ice thickness. The forecast's sea ice initial conditions showed biases, especially in sea ice thickness, and too-thick sea ice in regions that lost sea ice cover in observations were a likely source of forecast bias. In addition, this event highlights the impact that ocean waves may have on the sea ice pack, via their influence on the floe size distribution, lateral melt rates, and upper ocean mixing within the ice pack. Current forecast models do not include wave-sea ice interactions, but this is an area of active research that may lead to improved simulation and forecasts of rapid sea ice changes associated with extreme atmospheric and ocean wave conditions.

Data Availability Statement

NSIDC daily SIC data (Meier et al., 2013) are available at https://nsidc.org/data/g02202, ERA-5 data (Hersbach et al., 2020) are available at https://www.ecmwf.int/en/forecasts/dataset/ecmwf-reanalysis-v5, SMOS sea ice thickness data (Kaleschke et al., 2012) are available at https://smos-diss.eo.esa.int/oads/access/collection/L3_SIT_Open. AIRS data (Susskind et al., 2014) are available at www.airs.jpl.nasa.gov or by directly e-mailing Linette Boisvert (linette.n.boisvert@nasa.gov). CERES data (Wielicki et al., 1996) are available at https://asdc.larc.nasa.gov/project/CERES. ICESat-2 L3A sea ice height data (Kwok et al., 2020) are available at https://nsidc.org/data/icesat-2/data-sets. ECMWF forecast data are available at https://www.ecmwf.int/en/forecasts/dataset/operational-archive, copyright 2022 European Centre for Medium-Range Weather Forecasts (ECMWF).

Acknowledgments
The authors thank ECMWF for assistance with accessing their forecast data. The authors thank Cecilia Bitz, Robin Clancy, Steven Cavallo, Steffen Tietsche and three anonymous reviewers for helpful discussions, data access, and manuscript reviews. EBW was supported by NASA Grants 80NSSC20K0922, 80NSSC20K0959 and ONR-DRI Grant N00014-21-1-2490. MW, LB and CP were supported by NASA's Weather and Atmospheric Dynamics program (Grant 80NSSC20K0922), CH was supported by NASA Grant 80NSSC20K0959 and by Schmidt Futures, a philanthropic initiative that seeks to improve societal outcomes through the development of emerging science and technologies.

References

Asplin, M. G., Galley, R., Barber, D. G., & Prinsenberg, S. (2012). Fracture of summer perennial sea ice by ocean swell as a result of Arctic storms. *Journal of Geophysical Research*, *117*(C6). https://doi.org/10.1029/2011jc007221

Blanchard-Wrigglesworth, E., Donohoe, A., Roach, L. A., DuVivier, A., & Bitz, C. M. (2021). High-frequency sea ice variability in observations and models. *Geophysical Research Letters*, *48*(14), e2020GL092356. https://doi.org/10.1029/2020gl092356

Boisvert, L., Wu, D., Vihma, T., & Susskind, J. (2015). Verification of air/surface humidity differences from AIRS and ERA-Interim in support of turbulent flux estimation in the Arctic. *Journal of Geophysical Research: Atmospheres*, *120*(3), 945–963. https://doi.org/10.1002/2014jd021666

Boisvert, L. N., Markus, T., & Vihma, T. (2013). Moisture flux changes and trends for the entire Arctic in 2003–2011 derived from EOS Aqua data. *Journal of Geophysical Research: Oceans*, *118*(10), 5829–5843. https://doi.org/10.1002/jgrc.20414

Boisvert, L. N., Petty, A., & Stroeve, J. (2016). The impact of the extreme winter 2015/16 Arctic cyclone on the Barents–Kara seas. *Monthly Weather Review*, *144*(11), 4279–4287. https://doi.org/10.1175/mwr-d-16-0234.1

Cavallo, S. M., & Hakim, G. J. (2009). Potential vorticity diagnosis of a tropopause polar cyclone. *Monthly Weather Review*, *137*(4), 1358–1371. https://doi.org/10.1175/2008mwr2670.1

Clancy, R., Bitz, C. M., Blanchard-Wrigglesworth, E., McGraw, M. C., & Cavallo, S. M. (2022). A cyclone-centered perspective on the drivers of asymmetric patterns in the atmosphere and sea ice during Arctic cyclones. *Journal of Climate*, *35*(1), 73–89. https://doi.org/10.1175/jcli-d-21-0093.1

Hakim, G. J., & Canavan, A. K. (2005). Observed cyclone–anticyclone tropopause vortex asymmetries. *Journal of the Atmospheric Sciences*, *62*(1), 231–240. https://doi.org/10.1175/jas-3353.1

Hersbach, H., Bell, B., Berrisford, P., Hirahara, S., Horányi, A., Muñoz-Sabater, J., et al. (2020). The ERA5 global reanalysis [Dataset]. Quarterly Journal of the Royal Meteorological Society, *146*(730), 1999–2049. https://doi.org/10.1002/qj.3803

Horvat, C., Blanchard-Wrigglesworth, E., & Petty, A. (2020). Observing waves in sea ice with ICESat-2. *Geophysical Research Letters*, *47*(10), e2020GL087629. https://doi.org/10.1029/2020gl087629

Huang, Y., Taylor, P. C., Rose, F. G., Rutan, D. A., Shupe, M. D., Webster, M. A., & Smith, M. M. (2022). Toward a more realistic representation of surface albedo in NASA CERES-derived surface radiative fluxes: A comparison with the MOSAiC field campaign: Comparison of CERES and MOSAiC surface radiation fluxes. *Elementa: Science of the Anthropocene*, *10*(1), 00013. https://doi.org/10.1525/elementa.2022.00013

Kaleschke, L., Tian-Kunze, X., Maaß, N., Mäkynen, M., & Drusch, M. (2012). Sea ice thickness retrieval from SMOS brightness temperatures during the Arctic freeze-up period [Dataset]. Geophysical Research Letters, *39*(5). https://doi.org/10.1029/2012gl050916

Koyama, T., Stroeve, J., Cassano, J., & Crawford, A. (2017). Sea ice loss and Arctic cyclone activity from 1979 to 2014. *Journal of Climate*, *30*(12), 4735–4754. https://doi.org/10.1175/jcli-d-16-0542.1

Kwok, R., Cunningham, G., Markus, T., Hancock, D., Morison, J., Palm, S., et al. (2020). Atlas/icesat-2 l3a sea ice height, version 3 [Dataset]. NSIDC. Retrieved from https://nsidc.org/data/icesat-2/data-sets

Kwok, R., Markus, T., Kurtz, N., Petty, A., Neumann, T., Farrell, S., et al. (2019). Surface height and sea ice freeboard of the Arctic Ocean from ICESAT-2: Characteristics and early results. *Journal of Geophysical Research: Oceans*, *124*(10), 6942–6959. https://doi.org/10.1029/2019jc015486

Lindsay, R., Wensnahan, M., Schweiger, A., & Zhang, J. (2014). Evaluation of seven different atmospheric reanalysis products in the Arctic. *Journal of Climate*, *27*(7), 2588–2606. https://doi.org/10.1175/jcli-d-13-00014.1

Marko, J. R. (2003). Observations and analyses of an intense waves-in-ice event in the Sea of Okhotsk. *Journal of Geophysical Research*, *108*(C9), 3296. https://doi.org/10.1029/2001jc001214

McGraw, M. C., Blanchard-Wrigglesworth, E., Clancy, R. P., & Bitz, C. M. (2022). Understanding the forecast skill of rapid Arctic sea ice loss on subseasonal time scales. *Journal of Climate*, *35*(4), 1179–1196. https://doi.org/10.1175/jcli-d-21-0301.1

Meier, W., Fetterer, F., Savoie, M., Mallory, S., Duerr, R., & Stroeve, J. (2013). NOAA/NSIDC climate data record of passive microwave sea ice concentration, version 2 [Dataset]. National Snow and Ice Data Center. Retrieved from https://nsidc.org/data/g02202

Neu, U., Akperov, M. G., Bellenbaum, N., Benestad, R., Blender, R., Caballero, R., et al. (2013). Imilast: A community effort to intercompare extratropical cyclone detection and tracking algorithms. *Bulletin of the American Meteorological Society*, *94*(4), 529–547. https://doi.org/10.1175/bams-d-11-00154.1

Neumann, T. A., Martino, A. J., Markus, T., Bae, S., Bock, M. R., Brenner, A. C., et al. (2019). The ice, cloud, and land elevation satellite–2 mission: A global geolocated photon product derived from the advanced topographic laser altimeter system. *Remote Sensing of Environment*, *233*, 111325. https://doi.org/10.1016/j.rse.2019.111325

Park, H.-S., Lee, S., Son, S.-W., Feldstein, S. B., & Kosaka, Y. (2015). The impact of poleward moisture and sensible heat flux on Arctic winter sea ice variability. *Journal of Climate*, *28*(13), 5030–5040. https://doi.org/10.1175/jcli-d-15-0074.1

Rousset, C., Vancoppenolle, M., Madec, G., Fichefet, T., Flavoni, S., Barthélemy, A., et al. (2015). The Louvain-La-Neuve sea ice model LIM3.6: Global and regional capabilities. *Geoscientific Model Development*, *8*(10), 2991–3005. https://doi.org/10.5194/gmd-8-2991-2015

Schreiber, E. A., & Serreze, M. C. (2020). Impacts of synoptic-scale cyclones on Arctic sea-ice concentration: A systematic analysis. *Annals of Glaciology*, *61*(82), 139–153. https://doi.org/10.1017/aog.2020.23

Simmonds, I., Burke, C., & Keay, K. (2008). Arctic climate change as manifest in cyclone behavior. *Journal of Climate*, *21*(22), 5777–5796. https://doi.org/10.1175/2008jcli2366.1

Sorteberg, A., & Walsh, J. E. (2008). Seasonal cyclone variability at 70N and its impact on moisture transport into the Arctic. *Tellus A: Dynamic Meteorology and Oceanography*, *60*(3), 570–586. https://doi.org/10.1111/j.1600-0870.2007.00314.x

Stopa, J. E., Ardhuin, F., & Girard-Ardhuin, F. (2016). Wave climate in the Arctic 1992-2014: Seasonality and trends. *The Cryosphere*, *10*(4), 1605–1629. https://doi.org/10.5194/tc-10-1605-2016

Susskind, J., Blaisdell, J. M., & Iredell, L. (2014). Improved methodology for surface and atmospheric soundings, error estimates, and quality control procedures: The atmospheric infrared sounder science team version-6 retrieval algorithm [Dataset]. Journal of Applied Remote Sensing, *8*(1), 084994. https://doi.org/10.1117/1.jrs.8.084994

Taylor, P. C., Hegyi, B. M., Boeke, R. C., & Boisvert, L. N. (2018). On the increasing importance of air-sea exchanges in a thawing Arctic: A review. *Atmosphere*, *9*(2), 41. https://doi.org/10.3390/atmos9020041

Tian-Kunze, X., Kaleschke, L., Maaß, N., Mäkynen, M., Serra, N., Drusch, M., & Krumpen, T. (2014). SMOS-Derived thin sea ice thickness: Algorithm baseline, product specifications and initial verification. *The Cryosphere*, *8*(3), 997–1018. https://doi.org/10.5194/tc-8-997-2014

Waseda, T., Nose, T., Kodaira, T., Sasmal, K., & Webb, A. (2021). Climatic trends of extreme wave events caused by arctic cyclones in the Western Arctic Ocean. *Polar Science*, *27*, 100625. https://doi.org/10.1016/j.polar.2020.100625

Webster, M. A., Parker, C., Boisvert, L., & Kwok, R. (2019). The role of cyclone activity in snow accumulation on Arctic sea ice. *Nature Communications*, *10*(1), 1–12. https://doi.org/10.1038/s41467-019-13299-8

Wielicki, B. A., Barkstrom, B. R., Harrison, E. F., Lee, R. B., III, Smith, G. L., & Cooper, J. E. (1996). Clouds and the Earth's Radiant Energy System (CERES): An Earth observing system experiment, [Dataset]. Bulletin of the American Meteorological Society, *77*(5), 853–868. https://doi.org/10.1175/1520-0477(1996)077<0853:catere>2.0.co;2

Yamagami, A., Matsueda, M., & Tanaka, H. L. (2018). Medium-range forecast skill for extraordinary Arctic cyclones in summer of 2008–2016. *Geophysical Research Letters*, *45*(9), 4429–4437. https://doi.org/10.1029/2018gl077278